Journal of Materials Chemistry C

ROYAL SOCIETY OF CHEMISTRY

PAPER

View Article Online
View Journal | View Issue

Cite this: J. Mater. Chem. C, 2022, 10, 12715

Large-area SHG-CD probe intrinsic chirality in polycrystalline films†

Florian Ristow, [a] Kevin Liang, [b] Johannes Pittrich, [a] Jakob Scheffel, [a] Natalie Fehn, [b] Reinhard Kienberger, [a] Ulrich Heiz, [b] Aras Kartouzian *[b] and Hristo Iglev *[a]

Received 24th April 2022,
Accepted 31st July 2022

DOI: 10.1039/d2tc01700h

rsc.li/materials-c

We used second harmonic generation (SHG) spectroscopy to study the chiroptical properties of *R*-, *S*- and racemic (*RAC*-) 1,1′-bi-2-naphthol (BINOL) films with various thicknesses, incidence angles and degrees of crystallization in the film. The SHG intensity measured at 337 nm increases for thicker films and upon crystallization, while the extracted SHG-circular dichroism (SHG-CD) shows two different regimes depending on the size of the investigated sample area. The data measured at small beam areas, compared to the supramolecular domain size, show strong variation of SHG-CD values depending on the local crystalline structure. In contrast, the anisotropy values measured for beam areas larger than the domain size are almost independent of local sample morphology, film thickness and incidence angle. The SHG-CD values change their sign upon sample flipping or going from *R*- to *S*-BINOL. Most interestingly, the observed SHG-CD almost coincides with the value reported for molecular monolayers. Our study reveals that SHG-CD measured with large beam areas can nullify the in-plane anisotropy by averaging over many domains, and thus directly probes intrinsic chirality of the sample. Molecule- and enantiospecific SHG-CD values for BINOL were obtained: ±1.06 for *R*- and *S*-BINOL, and 0.01 for racemic BINOL.

Introduction

Chirality is a unique property, in which a system cannot coincide with its mirror image.[1] Chirality is of great importance in a variety of scientific fields like biology, chemistry, and pharmaceutics.[2–4] Recently, chiral materials have attracted increasing interest due to their potential application in sensorics, optoelectronics and spintronics.[5–7] At present, a variety of organic-only/organic–inorganic chiral films and nanostructures have been designed through self-assembly processes.[8,9] These chiral materials exhibit interesting physical properties such as circular dichroism (CD),[10–14] circularly polarized photoluminescence,[15] nonlinear optical effects,[2] ferroelectricity,[16] and bulk photovoltaic effects.[17] Chirality is often probed by CD spectroscopy, which is a system's difference in absorption for left and right circularly polarized light.[18] Unfortunately, the detection of optical activity in thin molecular films proves to be challenging since the weak CD signals can be easily influenced by the interference of linear dichroism and linear birefringence due to local crystalline structures.[19–21]

Typically, nonlinear optics facilitates enhanced sensitivity towards chiroptical features in the investigated sample.[22–28] Particularly, chiral sensitivity in second harmonic generation – circular dichroism (SHG-CD) can be enhanced by up to three orders of magnitude if the SHG wavelength is resonant with the molecular transitions. However, SHG requires a non-centrosymmetric structure due to the spatial asymmetry requirement of nonlinear electric susceptibility.[29] At interfaces, the symmetry is broken by a change of medium which makes SHG inherently surface-sensitive,[30–32] although accurate chiroptical investigations are challenging due to the very weak SHG signals from monolayers. In addition, asymmetry in a system can be introduced by electric field-poling, self-assembly[2,33] or simply by crystallization. For multi-layer crystallized films, the nonlinear response is enhanced,[3,34] yet some of these films are prone to morphological changes which further complicates chiroptical sensing.[35] Experiments performed by Verbiest and Kauranen have shown that SHG-CD can arise even in achiral samples with in-plane anisotropy due to supramolecular ordering.[36–38] Therefore, the sensitivity of SHG-CD towards the chirality of

[a] *Physik-Department E11, Technische Universität München, James-Franck-Str. 1, D-85748, Garching, Germany. E-mail: hristo.iglev@tum.de*
[b] *Catalysis Research Center and Chemistry Department, Chair of Physical Chemistry, Technische Universität München; Lichtenbergstr. 4, 85748, Garching, Germany. E-mail: aras.kartouzian@mytum.de*

† Electronic supplementary information (ESI) available: Polarization quality measurements, sample preparation procedure, SHG-intensity for varying fundamental beam sizes and power, development of in-plane anisotropy over time, sample region scanning with different beam sizes, theoretical considerations. See DOI: https://doi.org/10.1039/d2tc01700h

polycrystalline films is not obvious, considering the different contributions from chiral and achiral components of the nonlinear susceptibility tensor as well as obstruction due to supramolecular structural domains.[39–42]

Due to its simplicity, BINOL has often been used as a probe molecule.[35,43] BINOL consists of two 2-napthol units and is a widely used molecule for asymmetric reactions.[44] Usually, theoretical descriptions of nonlinear optical activity for this material are based on a coupled Lorentz-oscillator model which was also found to be in agreement with the reported experimental data.[33] Although, under resonant excitation, magnetic contributions are considered to be enhanced relative to electric ones,[45] BINOL[46,47] and its derivatives, such as binaphthyl-based polymer samples,[48] were shown to be well described within the electric dipole approximation. We specifically note that this is not true for all molecules as some materials, such as stilbene or collagen-fibrils, show dominance of these magnetic contributions.[49,50]

In this work, we report data on SHG-CD measured at 337 nm in BINOL films with various thicknesses, incidence angles and at different crystallization stages. The chosen wavelength lies just within a resonant absorption band[34] which enhances the nonlinear response of the sample.[51] Despite the challenges in experiment and theory, we show that SHG-CD measured with large beam areas can nullify the in-plane anisotropy by averaging over an ensemble of supramolecular domains, and thus directly probes intrinsic chiral properties of polycrystalline films. The obtained molecule- and enantiospecific SHG-CD values could serve as benchmarks for the corresponding samples.

Experimental section

A schematic sketch of the used experimental setup can be found in Fig. 1. A commercial Ti:Sapphire oscillator (Femtosource Rainbow™, Femtolasers) with sub 30 fs laser pulses at a repetition rate of 78 MHz was used. A wavelength range of λ_{exc} = 674 ± 20 nm of the laser spectrum was selected with a bandpass filter (F1) and used for excitation in all SHG experiment presented in this study. This beam was guided into a chirped mirror compensation system, which accounts for the dispersive optical elements in the optical path before the sample. A Pockels cell (BME Bergmann) modulates the linear input polarization, thus creating left circularly polarized (LCP) and right circularly polarized (RCP) pulse bursts, in an alternating manner for SHG-CD measurements. Control measurements shown in Fig. S1 (ESI†) verify the excellent circularity of >99% of the setup (for more details see the ESI†). For most of our measurements, we used a switching frequency of 1 Hz for the Pockels cell. The fundamental beam was suppressed after the sample *via* a low-pass filter (F2), and a low-noise photomultiplier tube (SPC, Hamamatsu H8259) was used for detection of the weak SHG signal. Spectral selection was achieved by a monochromator unit. The SHG-CD circular anisotropy factor can be written as the circular differential second harmonic intensity signal normalized to the averaged SHG-intensity:[27,52]

$$\text{SHG-CD} = 2\frac{I_{LCP} - I_{RCP}}{I_{LCP} + I_{RCP}} \quad (1)$$

Here, L_{LCP} and L_{RCP} refer to the experimentally measured second harmonic intensities with left and right circularly polarized incident beams, respectively. We introduce a coordinate system, in which the beam polarization plane (X, Y) serves as an absolute reference. The sample plane (x, y) can be rotated relative to the laboratory frame (X, Y), characterized by the in-plane (θ) and out-of-plane (ψ) angles, respectively, with ψ = 0 representing normal incidence.

Results and discussion

SHG anisotropy for various beam areas

Here, we present data on SHG-CD measured in various BINOL films for different illuminated beam areas A. Three samples: enantiopure *R*-, pure *S*- and racemic BINOL, with each having a thickness of ~500 nm, were prepared in accordance with the sample preparation procedure described in the ESI,† and stored at room temperature and ambient pressure for more than 7 days. Note, that our recent study on the crystallization dynamics of thin BINOL films[53,54] indicated that the complete phase transition from an isotropic solid solution towards a polycrystalline film concludes after approximately 3 days.

Transmission microscopy images of *R*- and *RAC*-BINOL measured in crossed-polarizer configuration are shown in Fig. 2a and b. The *R*-BINOL sample contains relatively larger supramolecular domains compared with *RAC*-BINOL due to

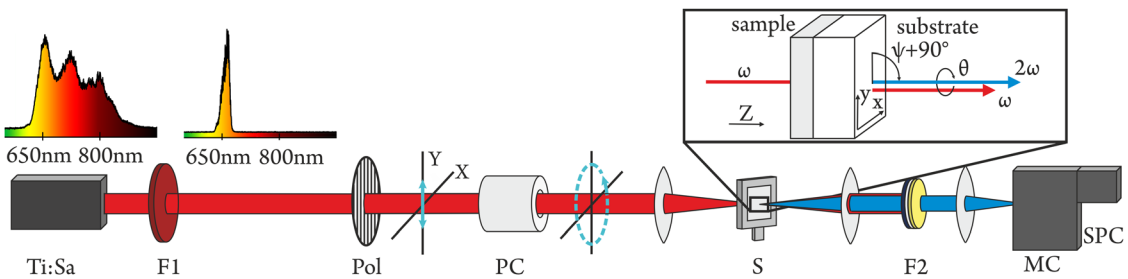

Fig. 1 Experimental setup. a Ti:Sapphire oscillator system (Ti:Sa) provides spectrally broad, ultrashort laser pulses. F1, F2: bandpass and low-pass filter. Pol: wire-grid polarizer. PC: a Pockels cell creates alternatingly right and left circularly polarized pulses. SH is generated from the sample and indicated in blue. S: sample. MC: monochromator. SPC: low-noise single-photon counting unit. The laser spectra before and after passing F1 are indicated.

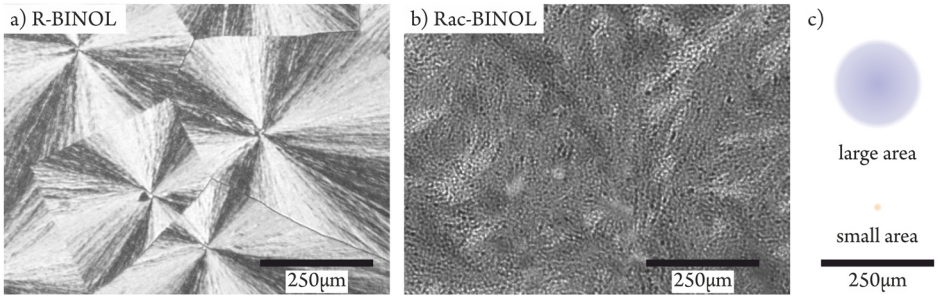

Fig. 2 (a and b) Are transmission microscopy images of *R*- and *RAC*-BINOL respectively. The supramolecular domains are larger for *R*-BINOL relative to *RAC*-BINOL. (c) True-to-scale illustration of the beam size for small (15 μm) and large area (225 μm) illumination used in the experiment.

their differences in morphology and purity. Fig. 2c gives a true-to-scale representation of the size of the fundamental laser beam in comparison to the size of the supramolecular domains. We evaluated the average diameter of the supramolecular domains in evaporated enantiopure *R*- and *S*-BINOL (∼255 μm).[53] Hence, the size of the beam can be related to the size of the crystalline domains. For small area illumination, a beam diameter significantly smaller (approx. 5%) than the domain size was used, while for large area illumination, the beam size (in our case 225 μm), is comparable to the domain size, which will be referred to as 'small *A*' and 'large *A*', respectively.

The beam size on the sample was controlled by adjusting the sample position relative to the focal point. It must be noted that when changing *A*, the intensity of fundamental incident radiation varies within the range of 1 MW cm^{-2} < I_ω < 1 GW cm^{-2}, hence the pulse energy density in our experiments varied from 30 nJ cm^{-2} and 30 μJ cm^{-2}. The chosen fundamental peak intensities are so low that they not only fall below the onset for multiphoton-absorption[53] ∼1.5 TW cm^{-2}, but also fall below the desorption threshold. We observed no significant desorption of material for any of our measurements. Otherwise, a decrease of SHG-intensity over time would be observed.[34]

The solid lines in Fig. 3 show the SHG-CD measurements for the different samples of BINOL, with each color representing a randomly chosen (*x*, *y*) position in the sample plane. The investigated samples show large positive and negative values for small *A* regardless of the enantiomeric constitution of the sample. The observation indicates that the anisotropy factors measured for small *A* do not stem from intrinsic chirality but mainly from the supramolecular in-plane orientation. As *A* is increased from small to large values, the SHG-CD shows a very large change in absolute value and can even change sign. The SHG-CD anisotropy factor stays constant within the measurement uncertainty after *A* exceeds a sample-specific value, tending to ∼ +0.7 and ∼−0.7 for *R*- and *S*-BINOL, respectively. A similar evolution of SHG-CD can be observed for racemic BINOL, of which the anisotropy value approaches zero for large beam areas.

An increase of *A* is accompanied by a decrease of nonlinear response, with which $I_{SHG} \sim I_\omega^2 \sim A^{-2}$. For convenience, an example for the evolution of I_{LCP} and I_{RCP} with *A* and the

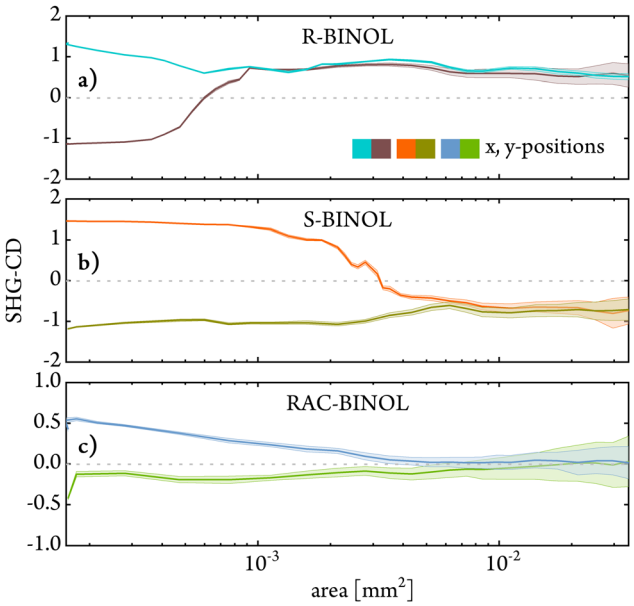

Fig. 3 SHG-CD values over sampling beam size area for (a) *R*-BINOL, (b) *S*-BINOL, and (c) racemic BINOL measured in two randomly chosen positions for each sample. The observed anisotropy values are obstructed for small beam areas, where in-plane contributions are dominant. Constant SHG-CD for large beam areas indicates a quasi-isotropy in the sample plane and therefore acquisition of an unobstructed, chiral SHG-CD signal.

quadratic dependence on the fundamental intensity is depicted in Fig. S2 in the ESI.† Essentially, the measured SHG count rates ($\propto I_{SHG} \cdot A$) become lower and the integrated intensities approach the systematic detector noise. Therefore, the signal to noise ratio (SNR) decreased from 100 : 1 for small values of *A*, to ∼5 : 1 for large values of *A*. The described change in SNR leads to significant increase of measurement uncertainty, as displayed by the line-plot shadows in Fig. 3.

In the following, we discuss the origin of two regimes: a varying, and a constant regime, for small values of *A* and large values of *A*, respectively. The crystallization of BINOL is mainly being driven by hydrogen-bonding between the hydroxyl-groups.[55–57] Enantiopure BINOL arranges in a trigonal crystal lattice, forming hexagonally shaped domains emanating from

crystallization seeds and racemic BINOL forms linear, elongated domains due to its orthorhombic lattice system.[58] Note that crystallization is particularly relevant in second harmonic generation spectroscopy, in which some polar order is required for nonlinear sensing of the film's bulk.[2,59] Although chiral molecules are inherently non-centrosymmetric, thin films of chiral molecules elude chiral sensing *via* SHG-CD spectroscopy due to an additional permutation symmetry of the hyperpolarizability tensor components.[2,59] However, as crystallization continues, additional centers of broken inversion symmetry arise, resulting in an increased nonlinear response of the system. This notion manifests itself as an in-plane contribution within the obtained anisotropy values. The emergence of crystallization centers in the film leads to anisotropy in the sample plane. As a result, molecular chiral films and even achiral will appear optically active in the nonlinear regime.[38,51,60]

Employing crystallized films to probe for nonlinear optical activity comes with an important drawback. Thin organic films such as BINOL oftentimes are polycrystalline, hence the sample is non-uniform within the (x, y)-plane. It has been proposed that these supramolecular domains are either chiral, achiral, or are a mixture of the two and their morphology is sample dependent.[61–63] When the illuminated beam area is small enough with respect to the size of the supramolecular domains, the in-plane anisotropies will play a significiant role in the obtained SHG-CD. Thus, the measured SHG-CD value heavily depends on the degree of isotropy within the illuminated sample area. In contrast, for measurements over large illumination areas, the sample will exhibit local in-plane anisotropy but will vary in their in-plane orientation, hence the sum of their contributions towards the overall anisotropy will average to zero. Accordingly, for measurements at large A, the sample behaves quasi-isotropically. In this case, the remaining nonlinear anisotropy originates from the intrinsic chirality in the sample. The quasi-isotropy is essential for further discussions, as it is associated with the property of cylindrical symmetry C_∞ within the sample plane. We emphasize that verifying the presence of cylindrical symmetry is experimentally desirable due to rotational invariance of the sample in the beam. The high degree of symmetry simplifies the theoretical considerations and discussions of data presented later in this work. For samples that are not quasi-isotropic at large scale, the intrinsic chirality can still be experimentally retrieved by averaging the nonlinear anisotropy over the in-plane angle θ.[42]

The requirement of a quasi-isotropy within the beam area is naturally opposed by the necessity of generating large SH signals and obtaining data with a good signal-to-noise ratio as $I_{\mathrm{SHG}} \propto A^{-2}$. For chiral sensing, it is therefore good practice to compromise between signal-to-noise and obstruction due to in-plane contributions.

SHG-CD in morphologically active films

We performed timed SHG-CD measurements to elucidate the influence of the sample's crystallization state on the obtained nonlinear anisotropy values. Fig. 4 shows typical SHG-CD data for *R*-BINOL (blue) and racemic BINOL (green) against the sample age. The data was acquired with large area illumination, so the SHG-CD values directly probe the intrinsic chirality in the film. We observed an increase in nonlinear response (data not shown) as the film underwent its phase transition. In contrast, the obtained SHG-CD values did not change within the uncertainty of the measurement, verifying the independence of the SHG-CD values from the phase transition within the sample.

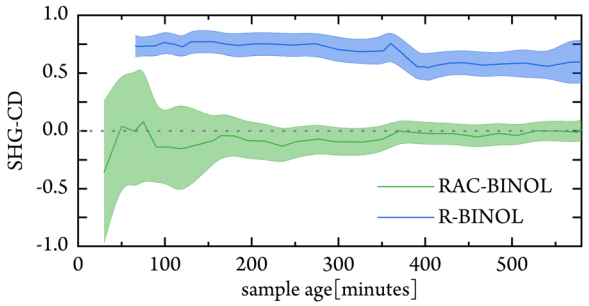

Fig. 4 Typical anisotropy values against sample age (minutes) for *R*-BINOL (blue) and *RAC*-BINOL (green) in two randomly chosen (x, y) positions. For both enantiomeric constitutions, the anisotropy value appears to be independent of the crystallization state of the sample.

The overall SHG-CD measured for racemic BINOL stays around zero and the value of ~ 0.7 is maintained over time for *R*-BINOL. For each sample, it can be inferred that similar anisotropy values are measured regardless of the crystallization state of the sample when measuring with large beam areas. The microscopy images shown in Fig. S3 (ESI†) illustrate that local in-plane anisotropy in the film highly increases throughout the crystallization process. For large area illumination however, the system can be considered as quasi-isotropic, and in-plane anisotropic contributions can be disregarded when measuring over multiple crystallite domains. The difference in the measured SNR with time in both samples can be attributed to the unequal crystal structures and concentrations of crystallization seeds.

Effect of the sample flipping on SHG-CD data

We investigated the influence of the illumination direction on the obtained SHG-CD values. Here, we considered two beam-to-sample configurations: illumination from the front and illumination from the back of the sample, as schematically displayed in Fig. 5a and b. In addition to the different illumination directions, the data measured for *R*-BINOL (5c and d), *S*-BINOL (e and f) and racemic BINOL (g and h) are shown with a small and large A relative to the size of the in-plane structures. For each side, measurements were performed at more than 400 randomly chosen sample positions, integrating over 3×10^8 laser pulses per position.

Quantitative comparison of the obtained mean-values for small and large A reveals good agreement, considering the width of the distribution. Histogram data in Fig. S4 (see ESI†), in which multiple beam sizes were used to map out the exact same sample region, additionally supports this averaging

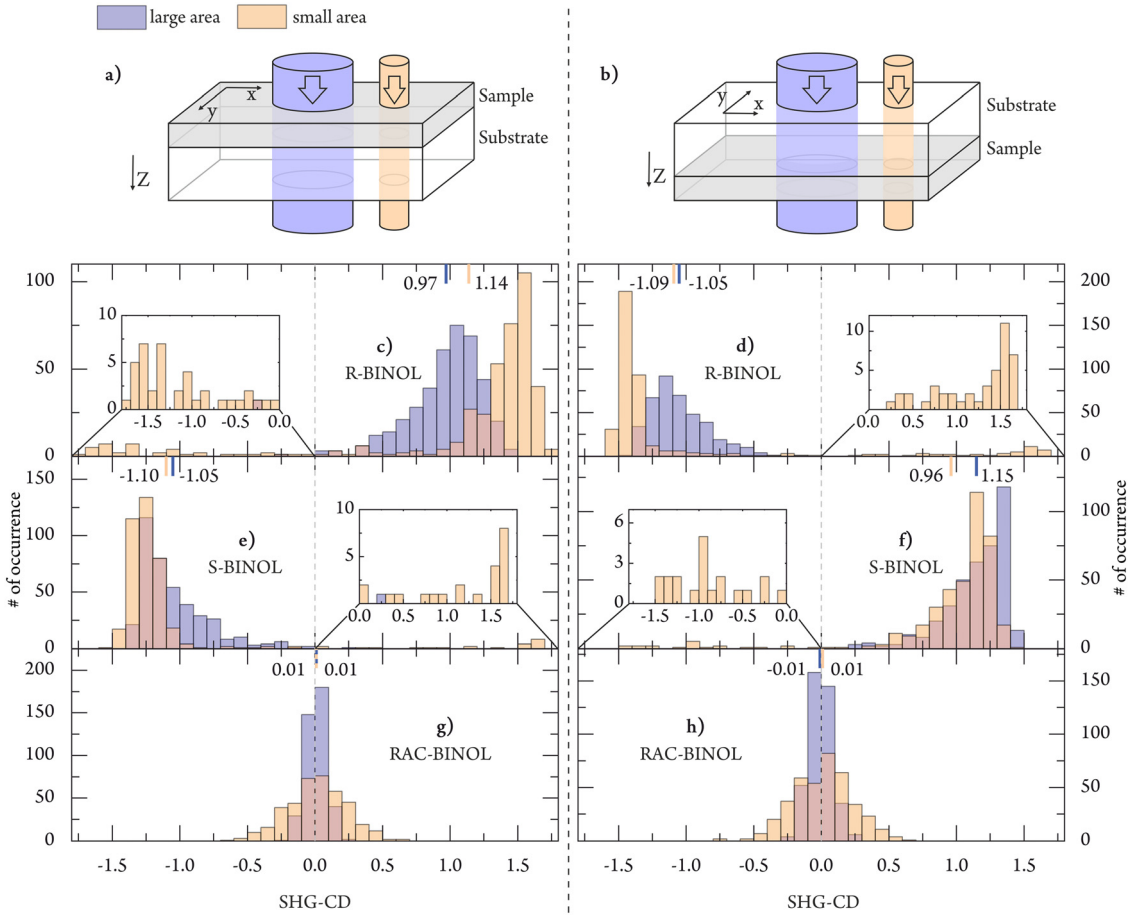

Fig. 5 Schematics for (a) front illumination and (b) back illumination. SHG-CD values obtained at λ_{exc} = 674 nm at 400 randomly chosen positions for: (c and d) *R*-BINOL; (e and f) *S*-BINOL; and (g and h) racemic BINOL. Reversal of the SHG-CD value can be observed for inversion of the sample with respect to the incident beam $\mathcal{J}$, and exchange of the enantiomer $\mathcal{E}$. For illumination with a small beam area relative to the size of the in-plane domains (yellow), in-plane contribution towards the SHG-CD do not average out and SHG-CD values span the full value set as indicated by the insets in (c–f). This is not the case for large area illumination (blue), for which in-plane contributions average out and the average SHG-CD directly probes chiral susceptibility. Regions for which the two histogram sets overlap are colored in red. The mean values of all value sets are displayed on the upper *x*-axis of each subplot.

argument. Evaluating all data in Fig. 5, we can give overall mean values for resonant excitation at 337 nm: 1.05 ± 0.36 and -1.07 ± 0.36 for front and back illumination respectively in *R*-BINOL, -1.07 ± 0.24 and 1.06 ± 0.23 for front and back respectively in *S*-BINOL, and 0.01 ± 0.12 and 0.01 ± 0.11 for front and back respectively in racemic BINOL. For large illumination areas *A*, *R*- and *S*-BINOL show reversal of the SHG-CD values, indicating the measurement's sensitivity towards chirality in the film. In the previous section, we attributed the obstruction of chirality measurements *via* SHG-CD to the emergence of in-plane contributions. This notion also shows itself in the statistical measurements. For small *A*, basically any SHG-CD value can be obtained for a randomly chosen position. This can be seen by the non-zero counts with opposite sign to the averaged SHG-CD value of the chiral samples in the inset-plots in Fig. 5c–f. The sign of the SHG-CD also shows reversal upon sample flipping (*i.e.*, inversion by rotating the sample around 180° around one of its in-plane axes).

We will use the analytical derivation of the SHG-CD within the plane-wave approximation, following works by Kauranen[64–66] and Schanne-Klein and colleagues[49] to explain the observed reversal of the SHG-CD upon exchange of the enantiomer and sample flipping. Here, expressions for both I_{LCP} and I_{RCP} are first derived from the nonlinear polarization and magnetization and then inserted into eqn (1). Schanne-Klein and colleagues have shown a simple expression for the linear and circular differential intensities, under the assumption that chiral and achiral components have a non-zero relative phase for resonant excitation. Similarly, Schmeltz and colleagues analytically derived a general expression for the nonlinear anisotropy of a sample with cylindrical symmetry C_∞.[50] Accordingly, the numerator of eqn (1) can be re-written as a linear combination of chiral and achiral susceptibility components:

$$\text{SHG-CD} \propto \sum_i \mathcal{C}_i \cdot \mathcal{A}_i \cdot \mathcal{P}_i \qquad (2)$$

Here, the $\mathcal{C}_i$ and $\mathcal{A}_i$ are linear combinations of chiral and achiral susceptibility components and can be of electric or magnetic origin. The phase delay constant p_i is the sinusoidal delay of the phases between the components $\mathcal{C}_i$ and $\mathcal{A}_i$. For resonant excitations, as in our case, one can argue that there

will be at least part of the signal with non-vanishing phase delay for all interfering chiral and achiral terms, hence $\mathcal{P}_i \neq 0$.[2,51] Per definition, the chiral components $\mathcal{C}_i$ vanish for achiral, racemic films without supramolecular order and is only nonzero for chiral films. Moreover, the ratio between chiral and achiral components is strongly sample specific, ranging from $\sim$1 : 10 for Langmuir-films[24] to $\sim$25 : 1 for BINOL.[35]

Byers and colleagues showed that their measurements on BINOL could be fully explained within the electric dipole approximation. In this case, magnetic and electric quadrupole components are considered negligible which simplifies calculations in eqn (2) (for more details see the ESI†). Note that precise knowledge of the magnitude of individual susceptibility tensor components is crucial for numerical simulations.[50] However, this is not necessary for the qualitative approach performed here, which simplifies the work to be done. Nevertheless, the majority of the tensor components vanish under consideration of the C_∞ – symmetry.[64]

In the following, we will look at two relevant properties of the tensor components for the transformations applied to the sample in the optical path, as performed in the measurements of SHG-CD above. The notable transformations are (i) an inversion of the sample relative to the beam and (ii) an exchange of the enantiomer. Similar considerations have been made before by Byers and colleagues[15] and Kauranen and colleagues.[22,65] We denote a sample-flipping operation in which the sample is rotated by 180° around the x-axis, with the "inversion-operator" $\mathcal{J} = \mathcal{J}_{z\to -z, y\to -y}$. Here, $\mathcal{C}_i = 0$ for achiral, racemic films and $\mathcal{C}_i \neq 0$ for chiral sample when averaging over many supramolecular domains. The chiral susceptibility in that case does necessarily have to be of molecular origin, but can also come from macroscopic structures in the sample. Independent of their origin, achiral components are antisymmetric with respect to inversion, while chiral components are symmetric. Hence, $\mathcal{A}_i \cdot \mathcal{J} = -\mathcal{A}_i$ and $\mathcal{C}_i \cdot \mathcal{J} = -\mathcal{C}_i$ and the SHG-CD changes sign correspondingly.

We also introduce an "exchange-operator" $\mathcal{E} = \mathcal{E}_{y\to -y}$, representing an exchange of the enantiomer, meaning that the enantiomeric constitution of the sample is reversed from dextrorotatory to levorotatory or *vice versa*. The exchange-operator is effectively a mirror operation for the enantiomeric excess ($\mathcal{C}_i$ will reverse sign after application of $\mathcal{E}$), hence $\mathcal{C}_i \cdot \mathcal{E} = -\mathcal{C}_i$. The exchange however does not affect achiral components, as they do not have enantiospecific character, hence $\mathcal{A}_i \cdot \mathcal{E} = \mathcal{A}_i$. Again, only one of the interfering components in the summands of eqn (2) changes sign upon transformation with ε, and SHG-CD changes sign correspondingly.

Reversal of the SHG-CD upon inversion can only be predicted when the sample is measured at large A. But even for the case of large area illumination, we do not necessarily observe reversal of SHG-CD when comparing the values in the same exact (x, y)-position for front and back illumination, which indicates residual in-plane anisotropy. For the data in Fig. 5c–h, only when looking at the sample macroscopically which is equivalent to averaging over many (x, y)-positions, the SHG-CD, within the electric dipole approximation, reverses when rotated around one of the in-plane axes.

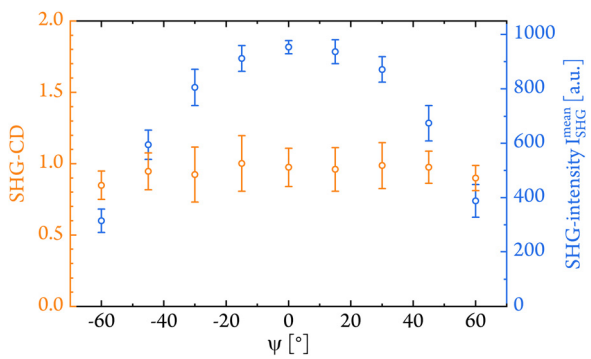

Fig. 6 SHG-CD (orange) and average SHG-intensity (blue) for different out-of-plane angles ψ measured on crystallized R-BINOL films. The obtained data with a sample size of more than 40 was averaged for each angle. The SHG-intensities follow a unique trigonometric angle-dependence, while the SHG-CD values coincide within the error bars.

Out-of-plane angle dependency

We studied the influence of the sample orientation relative to the polarization plane, called the out-of-plane angle ψ, on the observed large area SHG-CD values in a 500 nm thick film of R-BINOL. The results for the average intensity $I_{SHG}^{mean} = (I_{LCP} + I_{RCP})/2$ and SHG-CD values for each angle in front-illumination configuration can be seen in Fig. 6. It is evident that the average intensity follows a unique out-of-plane angle dependence. Recent study suggests that I_{SHG}^{mean} can be described as an even function which is a summation of trigonometric terms exponentiated up to the sixth order.[50] Qualitatively, the measured I_{SHG}^{mean} data fits this general form. Note that in general, SHG-intensities can show a variety of different out-of-plane angle behaviors, depending on the morphology of the film and the applied nonlinear sensing method.[67] Our data show a decrease of the SHG intensity as the sample was rotated away from normal incidence.

In contrast, when analyzing the dependency of SHG-CD on ψ, an almost constant value was observed within the measurement uncertainty. At best, a small decrease of the observable anisotropy values can be seen for a very tilted sample. Earlier studies on BINOL films by means of SHG and SFG performed by Hicks and Fischer[46,47] showed that electric dipolar contributions to the expected nonlinear response clearly dominate and, moreover, that the coupled-oscillator model[68] is applicable to BINOL. Interestingly in linear CD-spectroscopy, the observed CD-value can be obstructed by a non-molecular contribution called LDLB-term which describes the coupling of linear dichroism and linear birefringence.[19,20,69] Similar to SHG-CD, LDLB can also be described with the coupled oscillator model and as a consequence, a unique out-of-plane angle dependence is to be expected for the observed CD.[21,33] We emphasize that while the intensity is reduced due to an out-of-plane rotation of the sample with respect to the polarization plane of the incident beam, the SHG-CD value measured in the BINOL film

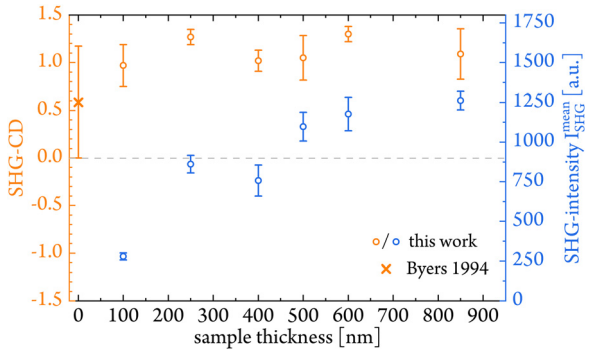

Fig. 7 SHG-CD for different thicknesses averaged over 80 positions for each angle. The values show weak dependency on the film thickness and an almost constant evolution within the error bars can be stated. We inserted an SHG-CD data point for monolayers taken from a study by Byers and colleagues.[22]

is not be greatly affected by this and still probes the intrinsic sample chirality.

Thickness dependency

Fig. 7 depicts the results of large-area SHG-CD measurements in crystallized *R*-BINOL films with varying thicknesses. The sample thickness was controlled with a custom-made quartz crystal microbalance (Inficon, IPN 750-207-G1). Note that some deviation in the sample thickness is possible, whereas the thickness uncertainty usually scales with the thickness itself.[53] An additional data point taken from a study by Byers and colleagues on *R*-BINOL monolayers adsorbed on the air–water interface was inserted for reference. For completeness, the measured SHG intensities I_{SHG}^{mean} are also shown in Fig. 7. The SHG-intensities increased with the film thickness in agreement with our previous studies.[34,35] In contrast, the SHG-CD values measured for various thicknesses match within the experimental accuracy. Most importantly, the measured SHG-CD values are similar to the number reported for the extreme case of a single molecular layer. The last comment should be taken with care, since the data sets cannot be necessarily compared with each other due to systematic differences in the experimental setup. In our measurements, we specifically emphasize the heavy dependence of the measured SHG-CD values with the quality of the circular polarization.

The observed invariance of the nonlinear anisotropy values with the sample thickness might not seem very surprising at first glance, since SHG-CD is normalized to the thickness. This idea, however, disregards the possible changes of the effective susceptibility tensor components accompanied by a change in thickness. In our previous study on freshly prepared, non-crystallized films, we already found evidence that the average out-of-plane orientation of the dipole moments changes when going from a monolayer to a thick, multi-layer film.[35] The current data suggests that the change in local crystal structure is rather insignificant for the observed large-area SHG-CD value. The measured value of $\sim$1.06 seems to directly probe the intrinsic chiral properties of the film and can serve as a benchmark for polycrystalline BINOL films.

Conclusion

In summary, we discuss the influence of in-plane anisotropy on the measured SHG-CD in crystallized films of chiral molecules. The SHG-CD data measured at small beam areas show strong variation depending on the local sample morphology, while the values measured for large beam areas are almost independent from local sample structure. When these in-plane features are averaged out by probing over multiple supramolecular domains, the SHG-CD data gives rise to a molecule-specific and enantiospecific signal. For an enantiopure film of chiral molecules, we observe inversion of the SHG-CD values when the sample is flipped or when the enantiomer is exchanged. We used theoretical considerations based on symmetry arguments to explain reversal of the sign in SHG-CD. The combination of experiment and theory reveals that, within resonant conditions and in the case of the electric dipole approximation, large-area SHG-CD directly probes the intrinsic chiral susceptibility, even in crystallized films with local in-plane anisotropy. We emphasize that the measured benchmark SHG-CD value of $\pm$1.06 (*R*- and *S*-BINOL) corresponds to more than a tripling in the SHG-yield when the illumination circular polarization is changed from right to left.

The idea of sensitivity to chirality *via* SHG-CD measurements of crystallized, multi-layer films is surprising considering the complex contributions from chiral and achiral tensor components as well as obstruction due to supramolecular domains. With the presented data on a simple reference system like BINOL, we prove that large-area SHG-CD probes intrinsic chiral properties in unordered polycrystalline films. Most importantly, this method shows high robustness against changes in the material thickness, large out-of-plane angle rotation, and morphological changes in the sample due to on-going crystallization. Our observation widens the range of possibilities for probing chirality by nonlinear sensing, since the requirements towards the sample itself are relatively relaxed. The sample can vary: from monolayer to multilayer films and/or from highly-controlled, morphologically active solid solutions to polycrystalline films.

Conflicts of interest

The authors declare no competing financial interest.

Acknowledgements

We acknowledge financial support by DFG through the projects KI 1304/8-3, KA 4166/2-1 and the Cluster of Excellence "e-conversion" EXC 2089/1-390776260.

References

1 L. W. T. Kelvin, *Baltimore lectures on molecular dynamics and the wave theory of light, CUP Archive*, 1904.
2 S. Sioncke, T. Verbiest and A. Persoons, *Mater. Sci. Eng., R*, 2003, **42**, 115–155.
3 M. Sun, L. Xu, A. Qu, P. Zhao, T. Hao, W. Ma, C. Hao, X. Wen, F. M. Colombari and A. F. de Moura, *Nat. Chem.*, 2018, **10**, 821–830.
4 E. Yashima, N. Ousaka, D. Taura, K. Shimomura, T. Ikai and K. Maeda, *Chem. Rev.*, 2016, **116**, 13752–13990.
5 M. Gao and W. Qin, *Adv. Opt. Mater.*, 2021, **9**, 2101201.
6 Y. Yang, R. C. Da Costa, M. J. Fuchter and A. J. Campbell, *Nat. Photonics*, 2013, **7**, 634–638.
7 H. Zheng, B. Ju, X. Wang, W. Wang, M. Li, Z. Tang, S. X. A. Zhang and Y. Xu, *Adv. Opt. Mater.*, 2018, **6**, 1801246.
8 J. Ma, H. Wang and D. Li, *Adv. Mater.*, 2021, **33**, 2008785.
9 B. Shen, Y. Kim and M. Lee, *Adv. Mater.*, 2020, **32**, 1905669.
10 J. Brahms and G. Spach, *Nature*, 1963, **200**, 72–73.
11 P. Jonkheijm, P. van der Schoot, A. P. Schenning and E. Meijer, *Science*, 2006, **313**, 80–83.
12 S. R. Martin and M. J. Schilstra, *Methods Cell Biol.*, 2008, **84**, 263–293.
13 G. Pescitelli, L. Di Bari and N. Berova, *Chem. Soc. Rev.*, 2014, **43**, 5211–5233.
14 A. P. Schenning, P. Jonkheijm, E. Peeters and E. Meijer, *J. Am. Chem. Soc.*, 2001, **123**, 409–416.
15 D. Di Nuzzo, L. Cui, J. L. Greenfield, B. Zhao, R. H. Friend and S. C. Meskers, *ACS Nano*, 2020, **14**, 7610–7616.
16 D. Liu, J. Wang, H. M. Jafri, X. Wang, X. Shi, D. Liang, C. Yang, X. Cheng and H. Huang, *npj Quantum Mater.*, 2022, **7**, 1–8.
17 D. S. Knoche, M. Steimecke, Y. Yun, L. Mühlenbein and A. Bhatnagar, *Nat. Commun.*, 2021, **12**, 1–8.
18 N. Berova, K. Nakanishi and R. W. Woody, *Circular dichroism: principles and applications*, John Wiley & Sons, 2000.
19 G. Albano, G. Pescitelli and L. Di Bari, *Chem. Rev.*, 2020, **120**, 10145–10243.
20 G. Albano, F. Salerno, L. Portus, W. Porzio, L. A. Aronica and L. Di Bari, *ChemNanoMat*, 2018, **4**, 1059–1070.
21 A. Salij, R. H. Goldsmith and R. Tempelaar, *J. Am. Chem. Soc.*, 2021, **143**, 21519–21531.
22 J. Byers, H. Yee, T. Petralli-Mallow and J. Hicks, *Phys. Rev. B: Condens. Matter Mater. Phys.*, 1994, **49**, 14643.
23 J. Byers, H. Yee and J. Hicks, *J. Chem. Phys.*, 1994, **101**, 6233–6241.
24 A. Ozcelik, R. Pereira-Cameselle, A. Von Weber, M. Paszkiewicz, M. Carlotti, T. Paintner, L. Zhang, T. Lin, Y.-Q. Zhang and J. Barth, *Langmuir*, 2018, **34**, 4548–4553.
25 M. J. Crawford, S. Haslam, J. Probert, Y. A. Gruzdkov and J. G. Frey, *Chem. Phys. Lett.*, 1994, **230**, 260–264.
26 J. M. Hicks, T. Petralli-Mallow and J. D. Byers, *Faraday Discuss.*, 1994, **99**, 341–357.
27 T. Petralli-Mallow, T. Wong, J. Byers, H. Yee and J. Hicks, *J. Phys. Chem.*, 1993, **97**, 1383–1388.
28 T. Verbiest, M. Kauranen, A. Persoons, M. Ikonen, J. Kurkela and H. Lemmetyinen, *J. Am. Chem. Soc.*, 1994, **116**, 9203–9205.
29 R. W. Boyd, *Nonlinear Optics*, Academic press, 2020.
30 A.-M. Pena, T. Boulesteix, T. Dartigalongue and M.-C. Schanne-Klein, *J. Am. Chem. Soc.*, 2005, **127**, 10314–10322.
31 Y. Shen, *Annu. Rev. Mater. Sci.*, 1986, **16**, 69–86.
32 V. Valev, *Langmuir*, 2012, **28**, 15454–15471.
33 D. M. Burland, R. D. Miller and C. A. Walsh, *Chem. Rev.*, 1994, **94**, 31–75.
34 F. Mortaheb, K. Oberhofer, J. Riemensberger, F. Ristow, R. Kienberger, U. Heiz, H. Iglev and A. Kartouzian, *Angew. Chem.*, 2019, **131**, 15832–15836.
35 P. Heister, T. Lünskens, M. Thämer, A. Kartouzian, S. Gerlach, T. Verbiest and U. Heiz, *Phys. Chem. Chem. Phys.*, 2014, **16**, 7299–7306.
36 M. Kauranen, S. Van Elshocht, T. Verbiest and A. Persoons, *J. Chem. Phys.*, 2000, **112**, 1497–1502.
37 T. Verbiest, M. Kauranen and A. Persoons, *J. Opt. Soc. Am. B*, 1998, **15**, 451–457.
38 T. Verbiest, M. Kauranen, Y. Van Rompaey and A. Persoons, *Phys. Rev. Lett.*, 1996, **77**, 1456.
39 R. L. Disch and D. Sverdlik, *Anal. Chem.*, 1969, **41**, 82–86.
40 J. H. Freudenthal, E. Hollis and B. Kahr, *Chirality*, 2009, **21**, E20–E27.
41 J. Schellman and H. P. Jensen, *Chem. Rev.*, 1987, **87**, 1359–1399.
42 S. Sioncke, S. Van Elshocht, T. Verbiest, A. Persoons, M. Kauranen, K. E. Phillips and T. J. Katz, *J. Chem. Phys.*, 2000, **113**, 7578–7581.
43 M. A. Kriech and J. C. Conboy, *J. Am. Chem. Soc.*, 2005, **127**, 2834–2835.
44 J. M. Brunel, *Chem. Rev.*, 2005, **105**, 857–898.
45 M. M. Kauranen, T. Verbiest, A. Persoons, E. Meijer, M. Teerenstra, A. Schouten, R. Nolte and E. Havinga, *Adv. Mater.*, 1995, **7**, 641–644.
46 J. D. Byers and J. M. Hicks, *Chem. Phys. Lett.*, 1994, **231**, 216–224.
47 P. Fischer, F. Wise and A. Albrecht, *J. Phys. Chem. A*, 2003, **107**, 8232–8238.
48 F. Hache, H. Mesnil and M.-C. Schanne-Klein, *J. Chem. Phys.*, 2001, **115**, 6707–6715.
49 M.-C. Schanne-Klein, F. Hache, T. Brotin, C. Andraud and A. Collet, *Chem. Phys. Lett.*, 2001, **338**, 159–166.
50 M. Schmeltz, C. Teulon, M. Pinsard, U. Hansen, M. Alnawaiseh, D. Ghoubay, V. Borderie, G. Mosser, C. Aimé and F. Légaré, *Optica*, 2020, **7**, 1469–1476.
51 G. J. Simpson, *J. Chem. Phys.*, 2002, **117**, 3398–3410.
52 A. von Weber, M. Jakob, E. Kratzer, A. Kartouzian and U. Heiz, *Chem. Phys. Chem.*, 2019, **20**, 134–141.
53 F. Ristow, J. Scheffel, X. Xu, N. Fehn, K. E. Oberhofer, J. Riemensberger, F. Mortaheb, R. Kienberger, U. Heiz and A. Kartouzian, *Chirality*, 2020, **32**, 1341–1353.
54 A. von Weber, D. C. Hooper, M. Jakob, V. K. Valev, A. Kartouzian and U. Heiz, *Chem. Phys. Chem.*, 2019, **20**, 62–69.
55 C. B. Aakeröy and A. M. Beatty, *Aust. J. Chem.*, 2001, **54**, 409–421.
56 G. R. Desiraju, *Acc. Chem. Res.*, 1996, **29**, 441–449.

57 K. Mori, Y. Masuda and S. Kashino, *Acta Crystallogr., Sect. C: Cryst. Struct. Commun.*, 1993, **49**, 1224–1227.
58 T. Lee and J. F. Peng, *Cryst. Growth Des.*, 2010, **10**, 3547–3554.
59 P. Fischer and F. Hache, *Chirality*, 2005, **17**, 421–437.
60 P. Fischer and A. Buckingham, *J. Opt. Soc. Am. B*, 1998, **15**, 2951–2957.
61 K.-H. Ernst, *Supramolecular Chirality*, 2006, 209–252.
62 Y.-y Xu, Y. Rao, D.-s Zheng, Y. Guo, M.-h Liu and H.-f Wang, *J. Phys. Chem. C*, 2009, **113**, 4088–4098.
63 I. Kuzmenko, H. Rapaport, K. Kjaer, J. Als-Nielsen, I. Weissbuch, M. Lahav and L. Leiserowitz, *Chem. Rev.*, 2001, **101**, 1659–1696.
64 M. Kauranen, T. Verbiest, J. J. Maki and A. Persoons, *J. Chem. Phys.*, 1994, **101**, 8193–8199.
65 M. Kauranen, T. Verbiest, S. Van Elshocht and A. Persoons, *Opt. Mater.*, 1998, **9**, 286–294.
66 J. J. Maki, T. Verbiest, M. Kauranen, S. V. Elshocht and A. Persoons, *J. Chem. Phys.*, 1996, **105**, 767–772.
67 J. Jerphagnon and S. Kurtz, *J. Appl. Phys.*, 1970, **41**, 1667–1681.
68 M. Belkin, Y. Shen and C. Flytzanis, *Chem. Phys. Lett.*, 2002, **363**, 479–485.
69 Y. Shindo, *Opt. Eng.*, 1995, **34**, 3369–3384.